

## Compact Size, High $\Sigma$ SFR: Defining Morphological Features of Ly $\alpha$ -Emitters

KEUNHO J. KIM <sup>1</sup>, ANAHITA ALAVI <sup>1</sup>, CHRISTOPHER SNAPP-KOLAS <sup>2</sup>, BRIAN SIANA <sup>2</sup>, JOHAN RICHARD <sup>3</sup>,  
HARRY TEPLITZ <sup>1</sup>, JAMES COLBERT <sup>1</sup>, VIHANG MEHTA <sup>1</sup>, ANA PAULINO-AFONSO <sup>4</sup> AND EROS VANZELLA <sup>5</sup>

<sup>1</sup>*IPAC, California Institute of Technology, 1200 E. California Boulevard, Pasadena, CA 91125, USA*

<sup>2</sup>*Department of Physics & Astronomy, University of California, Riverside, CA 92521, USA*

<sup>3</sup>*Univ Lyon, Univ Lyon1, Ens de Lyon, CNRS, Centre de Recherche Astrophysique de Lyon UMR5574, F-69230, Saint-Genis-Laval, France*

<sup>4</sup>*Instituto de Astrofísica e Ciências do Espaço, Universidade do Porto—CAUP, Rua das Estrelas, PT4150-762, Porto, Portugal*

<sup>5</sup>*INAF – OAS, Osservatorio di Astrofisica e Scienza dello Spazio di Bologna, via Gobetti 93/3, I-40129 Bologna, Italy*

### ABSTRACT

The mechanisms of Ly $\alpha$  photon escape are key to understanding galaxy evolution and cosmic reionization, yet remain poorly understood. We investigate the UV-continuum sizes of 23 Ly $\alpha$  emitters (LAEs) at Cosmic Noon ( $1.7 < z < 3.3$ ), extending previous size analyses to include fainter galaxies ( $M_{UV} \simeq -14$ ) using gravitational lensing. Our results show that these LAEs are unusually small for their luminosity, with a mean effective radius ( $r_{\text{eff}}$ ) of  $170 \pm 140$  pc. They follow a distinct size-luminosity relation, with an intercept at  $M_{UV} = -21$  approximately three times smaller than typical star-forming galaxies (SFGs) at similar redshifts. This relation, however, is consistent with that of low-redshift Green Pea galaxies, suggesting that LAEs maintain compact sizes across redshifts. We also find that Ly $\alpha$  equivalent width ( $\text{EW}(\text{Ly}\alpha)$ ) increases with decreasing  $r_{\text{eff}}$ , confirming previous findings. The small sizes of LAEs lead to high star formation surface densities ( $\Sigma\text{SFR} = 1 - 600 M_{\odot} \text{ yr}^{-1} \text{ kpc}^{-2}$ ), clearly separating them from typical SFGs in the  $\Sigma\text{SFR}$  vs.  $r_{\text{eff}}$  space. Given that high  $\Sigma\text{SFR}$  is linked to strong galactic outflows, our findings imply that compact morphology plays a key role in Ly $\alpha$  escape, likely facilitated by outflows that clear under-dense channels in the ISM. Thus, these results demonstrate that compact size and high  $\Sigma\text{SFR}$  can help identify Ly $\alpha$ -emitters.

### 1. INTRODUCTION

Ly $\alpha$ -emitters (LAEs) are a class of galaxies that emit prominent Ly $\alpha$  photons. Since Ly $\alpha$  emission line is usually generated by intense star formation activity and/or AGN, most LAEs have high star formation rate (SFR) for their stellar mass (i.e., specific star formation rate (sSFR)  $\gtrsim 10^{-8} \text{ yr}^{-1}$ ) and relatively young stellar population ages ( $\lesssim 50$  Myr) (e.g., Malhotra & Rhoads 2002; Gawiser et al. 2007; Pirzkal et al. 2007; Finkelstein et al. 2015a; Liu et al. 2023). However, because Ly $\alpha$  photons are resonantly scattered by neutral hydrogen and can be significantly absorbed by dust (e.g., Ahn et al. 2003; Chang et al. 2023), not all star-forming galaxies (SFGs) show Ly $\alpha$  emission. This means that for a galaxy to become a LAE, Ly $\alpha$  photons have to find a way to escape from star-forming regions within the galaxy all the way

to the intergalactic medium (IGM). So, which properties of LAEs make Ly $\alpha$  escape possible?

Understanding the escape process of Ly $\alpha$  photons is also important for deciphering the cosmic reionization processes in the early Universe ( $z > 6$ ). This is because both Ly $\alpha$  photons and ionizing photons (Lyman-continuum, LyC) generally require low column density of neutral hydrogen ( $N(\text{HI})$ ) and/or low amount of dust along their escape pathways, as clearly supported by radiative transfer models (e.g., Neufeld 1991; Verhamme et al. 2015; Chang et al. 2023). Numerous observations of LyC leakers across redshifts ( $0 \lesssim z \lesssim 4$ ) have confirmed such close connections between Ly $\alpha$  and LyC emission by finding that the majority of LyC leakers are indeed strong LAEs (Verhamme et al. 2015; de Barros et al. 2016; Izotov et al. 2016, 2018a; Steidel et al. 2018; Izotov et al. 2021; Gazagnes et al. 2020; Pahl et al. 2021; Flury et al. 2022). Thus, studying the physical properties of LAEs and understanding their Ly $\alpha$  (and potentially LyC) escape mechanisms have been important topics in the fields of galaxy evolution and cosmology,

respectively (e.g., Malhotra & Rhoads 2002; Malhotra et al. 2012; Rhoads et al. 2000, 2014; Finkelstein et al. 2015a; Oyarzún et al. 2017; Rivera-Thorsen et al. 2017, and references therein).

In particular, at high redshifts  $2 \lesssim z \lesssim 7$ , morphology analyses of bright ( $M_{UV} \lesssim -18$ ) LAEs show that the galaxies are mostly compact (with small effective radius  $r_{\text{eff}} \lesssim 1.5$  kpc), often with clumpy features shown in UV images (e.g., Dow-Hygelund et al. 2007; Overzier et al. 2008; Bond et al. 2009; Taniguchi et al. 2009; Gronwall et al. 2011; Bond et al. 2012; Malhotra et al. 2012; Jiang et al. 2013; Paulino-Afonso et al. 2018; Shibuya et al. 2019; Ritondale et al. 2019; Reddy et al. 2022; Liu et al. 2023). Based on the approximately constant physical sizes of LAEs over a wide span of redshift ( $2 \lesssim z \lesssim 6$ ), Malhotra et al. (2012) suggested that the compact morphology of LAEs is a crucial condition for a galaxy to become a LAE. This idea is qualitatively consistent and further supported by later analytic calculations on morphologically compact conditions (i.e., small  $r_{\text{eff}}$  and high star formation surface density  $\Sigma\text{SFR}$ ) for LAEs and LyC leakers by Cen (2020).

Later studies (i.e., Izotov et al. 2016, 2018a; Kim et al. 2020, 2021) extended the morphology analysis of LAEs to low redshift ( $z \sim 0.3$ ) based on a sample of ‘‘Green Pea’’ galaxies. The studies confirmed that the typical size of low- $z$  LAEs is similar to those of high- $z$  counterparts rather than showing a redshift-dependent size growth seen in typical (continuum-selected) SFGs (e.g., Shen et al. 2003; van der Wel et al. 2014; Shibuya et al. 2015), corroborating the idea about the non-evolving characteristic sizes of LAEs and the importance of compact size in Ly $\alpha$  emission from a galaxy.

In this paper, we extend previous size analyses of LAEs to fainter UV luminosity ( $M_{UV} \simeq -14$ ) by leveraging the gravitational lensing effects of the foreground clusters. By extending a UV-luminosity range towards faint galaxies, our analysis reveals the morphological properties of faint LAEs and investigates whether the faint LAEs also show distinctly small sizes compared to typical SFGs, as shown in the relative bright range ( $M_{UV} \lesssim -18$ ), or show substantially different morphological properties such as diffuse extended structures.

We also investigate the connection between Ly $\alpha$  emission properties (e.g., Ly $\alpha$  equivalent width) and the UV size to study more general aspects of the relation between Ly $\alpha$  escape and UV continuum size.

Section 2 describes our galaxy sample and procedures for UV size and luminosity measurements. In Section 3, we present our results. We discuss the size and luminosity properties of our sample LAEs and compare them with other types of galaxies in Section 4. We summarize

our conclusions in Section 5. Throughout this paper, we adopt the AB magnitude system and the  $\Lambda$ CDM cosmology of  $(H_0, \Omega_m, \Omega_\Lambda) = (70 \text{ kms}^{-1} \text{ Mpc}^{-1}, 0.3, 0.7)$ .

## 2. SAMPLE SELECTION AND ANALYSIS

### 2.1. LAE Sample

We define a sample of 23 LAEs drawn from Snapp-Kolas et al. (2023), where the LAEs were identified during the Keck/LRIS spectroscopy follow-up campaign. This campaign was designed to target photometrically-selected  $1.5 < z_{\text{phot}} < 3.5$  lensed galaxies with apparent magnitude brighter than  $m_{F625W} < 26.3$ . The target fields of our sample galaxies comprise three galaxy clusters: MACSJ0717, MACSJ1149, and Abell 1689. The two MACS clusters are part of the Hubble Frontier Field (HFF) clusters (Lotz et al. 2017). From the Keck observations, 23 LAEs with the rest-frame equivalent width of Ly $\alpha$  ( $\text{EW}(\text{Ly}\alpha) > 20 \text{ \AA}^1$ ) were found at spectroscopic redshifts  $1.7 < z_{\text{spec}} < 3.3$ , with a median redshift of 2.43.

The median lensing magnification factor  $\mu$  of the sample galaxies is 8.8, representing the ratio of the observed flux to the intrinsic flux without lensing. This value is derived from strong lensing models for the clusters as reported by Limousin et al. (2007), Limousin et al. (2016), and Jauzac et al. (2016) for Abell 1689, MACSJ0717, and MACSJ1149, respectively. The R.A. and Dec. coordinates and the lensing magnification factor of the sample galaxies are listed in Table 1. We refer the readers to Snapp-Kolas et al. (2023) for further details about our sample LAEs.

### 2.2. Size and Luminosity Measurements

We measure the UV size of our sample LAEs by fitting their 2D surface brightness profiles. As described below, we utilize deep HST images that enable us to securely measure the UV size of our sample galaxies down to faint UV luminosity ( $\simeq 0.01L_*$ , where  $L_*$  is the characteristic UV luminosity corresponding to  $M_{UV} = -21$  at  $z = 3$ , Reddy & Steidel 2009; Steidel et al. 2018). Thus, our analysis covers a wide range of UV luminosities for LAEs, including both bright ( $0.3 - 1 L_{UV}/L_*$ ) and faint ( $0.12 - 0.3 L_{UV}/L_*$ ) luminosities. Specifically, we use the HST Advanced Camera for Surveys/Wide Field Camera (ACS/WFC) F606W and F625W images for the sample galaxies in the two HFF clusters and

<sup>1</sup> This definition of a LAE with  $\text{EW}(\text{Ly}\alpha) > 20 \text{ \AA}$  is commonly adopted in the literature (e.g., Steidel et al. 2011; Hathi et al. 2016).

**Table 1.** The Physical Properties of the Sample LAEs.

Galaxy ID	R.A. (deg)	Decl. (deg)	$z_{\text{spec}}$	$M_{\text{UV}}$	$r_{\text{eff}}$ ( pc)	$n_s$	$b/a$	EW(Ly $\alpha$ ) (Å)	$\mu$
A1689-257	197.8601135	-1.358672653	1.705	$-17.62^{+0.05}_{-0.05}$	$116.8^{+5.07}_{-4.74}$	$1.0 \pm 0.12$	$0.2 \pm 0.03$	$99.7^{+16.1}_{-16.1}$	$6.19 \pm 0.25$
A1689-280	197.8828396	-1.357248833	1.705	$-17.18^{+0.19}_{-0.21}$	$178.67^{+25.52}_{-20.77}$	$3.82 \pm 0.2$	$0.13 \pm 0.01$	$35.1^{+2.4}_{-2.4}$	$22.08 \pm 3.55$
A1689-539	197.8740075	-1.352060819	3.046	$-18.59^{+0.08}_{-0.08}$	$141.53^{+6.45}_{-5.91}$	$0.5 \pm 0.04$	$0.16 \pm 0.01$	$22.3^{+3.4}_{-3.4}$	$8.47 \pm 0.63$
A1689-540	197.8709266	-1.35206099	2.546	$-17.45^{+0.09}_{-0.09}$	$77.47^{+6.0}_{-5.47}$	$1.32 \pm 0.34$	$0.49 \pm 0.06$	$67.2^{+7.37}_{-8.74}$	$9.04 \pm 0.61$
A1689-830	197.8540603	-1.344897081	2.666	$-18.97^{+0.06}_{-0.06}$	$93.45^{+4.97}_{-4.72}$	$2.13 \pm 0.2$	$0.1 \pm 0.03$	$76.6^{+2.30}_{-2.27}$	$5.6 \pm 0.27$
A1689-920	197.8954312	-1.34277496	2.546	$-16.34^{+0.15}_{-0.17}$	$23.27^{+3.49}_{-3.0}$	$5.62 \pm 1.22$	$0.11 \pm 0.05$	$65.8^{+7.43}_{-6.28}$	$25.12 \pm 3.0$
A1689-946	197.8954312	-1.34277496	2.287	$-15.41^{+0.35}_{-0.39}$	$42.27^{+13.44}_{-10.63}$	$8.0 \pm 4.93$	$0.58 \pm 0.12$	$118.2^{+30.16}_{-24.46}$	$30.2 \pm 6.0$
A1689-1000	197.8777216	-1.34024891	2.665	$-13.69^{+11.22}_{-7.49}$	$9.47^{+288.61}_{-9.41}$	$1.03 \pm 0.05$	$0.11 \pm 0.02$	$66.7^{+2.82}_{-2.71}$	$991 \pm 29824$
A1689-1037	197.8966616	-1.34028896	1.703	$-15.79^{+0.35}_{-0.5}$	$135.0^{+38.08}_{-22.44}$	$2.09 \pm 0.12$	$0.49 \pm 0.02$	$23.4^{+3.69}_{-3.54}$	$43.25 \pm 15.46$
A1689-1117	197.895417	-1.33847996	2.546	$-10.03^{+12.9}_{-8.42}$	$19.18^{+907.64}_{-19.13}$	$0.5 \pm 0.22$	$0.13 \pm 0.03$	$216.5^{+62.94}_{-26.19}$	$2334 \pm 141885$
A1689-1197	197.8737117	-1.335775444	1.706	$-17.68^{+0.14}_{-0.16}$	$186.89^{+16.97}_{-14.09}$	$2.65 \pm 0.11$	$0.41 \pm 0.01$	$43.4^{+2.30}_{-2.30}$	$17.22 \pm 2.15$
A1689-40000	197.8633348	-1.347704975	1.837	$-17.82^{+0.13}_{-0.14}$	$174.09^{+17.03}_{-17.03}$	$3.15 \pm 0.16$	$0.27 \pm 0.01$	$107.2^{+2.63}_{-2.61}$	$25.82 \pm 2.1$
A1689-40011	197.8651121	-1.359898194	2.594	$-17.54^{+0.16}_{-0.19}$	$189.55^{+24.62}_{-20.55}$	$2.42 \pm 0.2$	$0.34 \pm 0.01$	$160.4^{+8.78}_{-8.19}$	$20.14 \pm 2.59$
MACSJ1149-1098	177.4065351	22.39286171	1.895	$-20.26^{+0.09}_{-0.1}$	$203.06^{+1.9}_{-1.9}$	$5.17 \pm 0.21$	$0.05 \pm 0.0$	$52.1^{+3.49}_{-3.63}$	$18.71^{+1.40}_{-1.78}$
MACSJ1149-1721	177.4201963	22.40213713	2.095	$-18.25^{+0.03}_{-0.04}$	$276.83^{+14.09}_{-13.05}$	$2.58 \pm 0.36$	$0.37 \pm 0.03$	$197.5^{+33.45}_{-28.54}$	$1.58^{+0.02}_{-0.02}$
MACSJ1149-1856	177.3840617	22.40503821	2.035	$-16.65^{+0.24}_{-0.24}$	$203.06^{+62.98}_{-51.78}$	$8.00 \pm 4.75$	$0.70 \pm 0.10$	$67.5^{+215.72}_{-96.03}$	$2.83^{+0.17}_{-0.12}$
MACSJ1149-2520	177.4068209	22.41625532	2.422	$-19.59^{+0.07}_{-0.07}$	$176.01^{+10.2}_{-9.8}$	$8.00 \pm 1.09$	$0.85 \pm 0.03$	$110.1^{+18.73}_{-13.53}$	$1.56^{+0.06}_{-0.04}$
MACSJ1149-2533	177.4161338	22.41659674	3.227	$-19.99^{+0.03}_{-0.03}$	$590.16^{+12.27}_{-12.29}$	$0.81 \pm 0.03$	$0.45 \pm 0.01$	$41^{+15.73}_{-14.26}$	$1.32^{+0.02}_{-0.02}$
MACSJ1149-2620	177.4120997	22.4187921	2.491	$-17.92^{+0.04}_{-0.04}$	$276.79^{+16.63}_{-16.16}$	$1.36 \pm 0.29$	$0.21 \pm 0.04$	$25.9^{+34.36}_{-21.54}$	$1.34^{+0.03}_{-0.03}$
MACSJ1149-2761	177.4116563	22.42309318	3.31	$-19.78^{+0.04}_{-0.04}$	$479.89^{+15.27}_{-14.7}$	$1.78 \pm 0.12$	$0.69 \pm 0.02$	$50^{+43.59}_{-32.32}$	$1.33^{+0.03}_{-0.03}$
MACSJ0717-744	109.3640224	37.73280612	3.042	$-19.18^{+0.02}_{-0.02}$	$268.13^{+6.37}_{-6.34}$	$2.28 \pm 0.14$	$0.1 \pm 0.01$	$61.9^{+17.61}_{-15.62}$	$1.70^{+0.02}_{-0.01}$
MACSJ0717-1034	109.3653315	37.73842898	2.441	$-18.67^{+0.03}_{-0.03}$	$38.34^{+3.72}_{-3.7}$	$7.3 \pm 1.44$	$0.12 \pm 0.05$	$63.2^{+13.37}_{-11.75}$	$1.88^{+0.02}_{-0.01}$
MACSJ0717-1170	109.3985407	37.74149598	1.859	$-16.88^{+0.14}_{-0.16}$	$83.0^{+7.74}_{-6.37}$	$2.41 \pm 0.19$	$0.5 \pm 0.02$	$73.6^{+5.52}_{-5.25}$	$11.90^{+2.14}_{-0.95}$

the Abell cluster, respectively. The images trace the rest frame UV-continuum (1500 – 2200 Å) at redshifts  $1.7 < z < 3.3$ . The F606W images are obtained from the HFF science products<sup>2</sup>. The images have a total exposure time of 27,015 and 24,816 seconds for MACSJ0717 and MACSJ1149 clusters, respectively, with a common pixel scale of  $0.03''$  pixel<sup>-1</sup>. The F625W image for the Abell 1689 cluster was originally obtained from the HST-GO-9289 (PID: H. Ford) and has a total exposure time of 9500 seconds and a pixel scale of  $0.04''$  pixel<sup>-1</sup>. The F625W image we use in this paper was processed and presented in Alavi et al. (2014, 2016), and we refer the reader to these papers for further details on the image processing.

We employ the GALFIT software (Peng et al. 2002, 2010) to measure the size of our sample galaxies by fitting their 2D surface brightness profiles with a Sérsic light profile model (Sérsic 1968). We fit the image region centered on a galaxy, ensuring that the image size

is sufficient to capture the galaxy’s light while also allowing for an accurate estimation of the background sky light. The point spread function (PSF) effect is taken into account in our surface brightness fitting by incorporating the PSF star image during the GALFIT procedure. We generated a PSF image for each cluster by selecting the unsaturated and isolated stars and stacking them using the StarFinder (Diolaiti et al. 2000) procedure.

We put constraints on the fitting ranges of the structural parameters to prevent the fitting from resulting in unphysical results (e.g., unphysically large effective radius). Such constraints have been often adopted in other studies employing the least- $\chi^2$  fit algorithm for galaxy surface brightness such as GALFIT (e.g., Peng et al. 2002; van der Wel et al. 2012; Kim et al. 2016; Shibuya et al. 2019). Specifically, we consider the following fitting ranges: major-axis effective radius  $r_{\text{eff}} > 0.5$  pixels; Sérsic index  $0.5 < n < 8$ ; axis-ratio  $b/a > 0.1$ , which are qualitatively similar to those of van der Wel et al. (2012).

We correct for lensing magnification to the size and luminosity measured in the image plane by using the magnification factor derived from the public strong lens

<sup>2</sup> <https://archive.stsci.edu/prepds/frontier/>

models described in Section 2.1. For a summary of the lens models used here, we refer the reader to Alavi et al. (2016).

For the majority of sample galaxies (that is, 21 out of 23), their morphology is appreciably compact. Thus, a simple lensing correction via dividing the size and luminosity by  $(\sqrt{\mu})$  and  $\mu$ , respectively, can be regarded as a feasible way to estimate the overall intrinsic properties of a galaxy. This is to keep the surface brightness fixed, because lensing does not change it (e.g., Sharon et al. 2022).

The remaining sample galaxies are two magnified arcs (Galaxy IDs: MACSJ1149-1098 and A1689-40000), for which we measure their sizes directly on the source-plane reconstructed images. This approach is necessary because their image-plane counterparts exhibit highly elongated arc morphologies, making the simple lensing corrections highly uncertain.

We correct the galaxy magnitude for the mean wavelength of 1800 Å by adopting the UV spectral slope measured using the best SED fitting technique discussed in A. Alavi, 2024 (submitted to ApJ). The best SED fits are done similarly to what is presented in Alavi et al. (2016). In brief, the best SEDs for two HFF clusters, MACSJ0717 and MACSJ1149, utilize publicly available deep data in 10 *HST* broad-band filters, including F225W, F275W, F336W, F435W, F606W, F814W, F105W, F125W, F140W, and F160W. The UV data are sourced from *HST* program IDs 15940 (F225W; PI: Ribeiro) and 13389 (F275W and F336W; PI: B. Siana), while the optical and NIR data are obtained from *HST* program ID 13495 (PI: Lotz). For Abell 1689, we utilize publicly accessible photometric data in 8 *HST* bands, specifically F225W, F275W, F336W, F475W, F625W, F775W, F814W, and F850LP. The UV data for A1689 are associated with program IDs 12201 and 12931 (PI: B. Siana).

The physical properties of our sample galaxies are provided in Table 1.

### 3. RESULTS

#### 3.1. Size Distribution of LAEs at Cosmic Noon $1.7 < z < 3.3$

The main goal of this paper is to investigate the UV-continuum size of LAEs and compare the typical size of LAEs with that of continuum-selected star-forming galaxies (i.e., Lyman Break Galaxies and/or photometrically selected star-forming galaxies). Our analysis extends previous size analyses of LAEs to fainter UV luminosity ( $M_{UV} \simeq -14$ ) by leveraging the gravitational lensing effects of the foreground clusters.

The left panel of Figure 1 shows the size distribution of our sample LAEs. Compared to the typical PSF FWHM of the *HST* images, the sizes of sample LAEs are mostly resolved due to the high spatial-resolution of the *HST* images. The size is corrected for lensing magnification, and measured as the circularized effective size  $r_{\text{eff}}$  (that is,  $r_{\text{eff}} = r_{\text{maj}} \times \sqrt{b/a}$ , where  $b/a$  and  $r_{\text{maj}}$  are the galaxy axis ratio and effective radius along major-axis, respectively); This size definition is commonly adopted in other studies (e.g., van der Wel et al. 2014; Shibuya et al. 2015; Kim et al. 2021; Nedkova et al. 2024), which allows us to compare our size measurements with the literature in a consistent manner.

The distribution shows the mean size of 170 pc and the associated standard deviation of 140 pc of the sample galaxies, with a long tail toward large sizes up to  $\simeq 0.6$  kpc. As we will further discuss below, our sample LAEs' size distribution indicates a very small typical size for their UV luminosity compared to typical (i.e., including all types of) star-forming galaxies with similar UV luminosity at similar redshifts.

Specifically, our UV bright ( $0.3 - 1 L_{UV}/L_*$ ) sub-sample galaxies show a factor of  $\sim 4$  smaller average size of  $0.42 \pm 0.16$  kpc compared to those ( $1.4 \lesssim r_{\text{eff}} \lesssim 2$  kpc) of the photometrically selected star-forming galaxies (SFGs) and Lyman Break Galaxy (LBG) counterparts at similar redshifts  $z = 2 - 3$  (Bouwens et al. 2004; van der Wel et al. 2014; Shibuya et al. 2015; Ribeiro et al. 2016; Nedkova et al. 2024). This trend of the small typical size of the sample LAEs is found regardless of specific UV luminosity bins; Consistent with the bright sub-sample, our faint ( $0.12 - 0.3 L_{UV}/L_*$ ) sub-sample galaxies also exhibits small sizes, with an average size of  $0.30 \pm 0.18$  kpc. This contrasts with the average size of  $\simeq 0.8$  kpc of the SFGs and LBGs counterparts at similar redshifts. (e.g., van der Wel et al. 2014; Shibuya et al. 2015).

While the sizes of our sample LAEs are smaller compared to typical SFGs at similar redshifts, they are consistent with the typical sizes of LAEs across a wide range of redshift  $0.1 < z < 6$ , where the reported size ranges between  $r_{\text{eff}} = 0.3 - 1$  kpc (e.g., Dow-Hygelund et al. 2007; Overzier et al. 2008; Bond et al. 2009; Taniguchi et al. 2009; Bond et al. 2012; Malhotra et al. 2012; Jiang et al. 2013; Paulino-Afonso et al. 2018; Shibuya et al. 2019; Ritondale et al. 2019; Kim et al. 2021; Flury et al. 2022; Reddy et al. 2022; Liu et al. 2023; Ning et al. 2024).

The right panel of Figure 1 shows the UV luminosity distribution of our sample galaxies, ranging from bright ( $M_{UV} \simeq -20$  to faint ( $M_{UV} \simeq -14$ ) luminosities. The median UV luminosity of these galaxies is -17.7. The

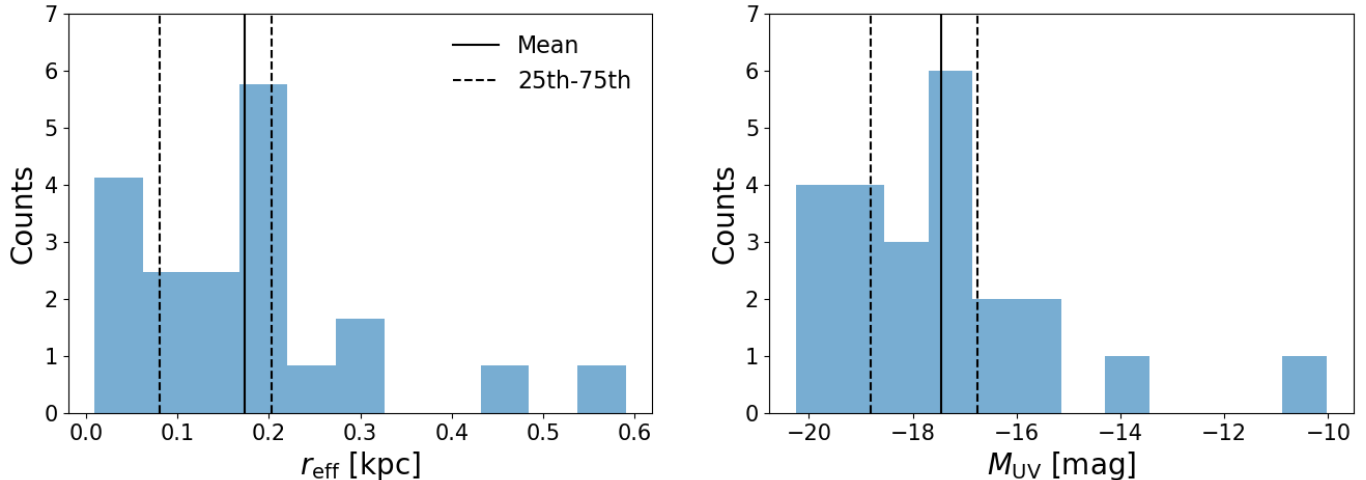


**Figure 1. Left:** UV-continuum size (corrected for lensing) of our sample LAEs at  $1.7 < z < 3.3$ . The mean size (solid vertical line) and the interquartile range (dashed vertical lines) are  $170^{+30}_{-90}$  pc. **Right:** The lensing-corrected UV luminosity distribution for the LAEs. The median UV luminosity is  $-17.66^{+0.91}_{-1.14}$  magnitudes, with the interquartile range represented in the same manner as in the left panel.

luminosities are corrected for lensing-magnification ( $\mu$ ), as described in Section 2.

### 3.2. UV Size-luminosity Relations of LAEs

At all redshifts, galaxies show a tight relation between their size and luminosity (similarly stellar mass) (e.g., Bouwens et al. 2004; van der Wel et al. 2014; Shibuya et al. 2015; Morishita et al. 2024; Nedkova et al. 2024), which is also supported by theoretical galaxy disk formation models (e.g., Fall & Efstathiou 1980; Barnes & Efstathiou 1987; Mo et al. 1998; Wyithe & Loeb 2011; Liu et al. 2017). The size-luminosity relation is often parameterized as a power-law with a slope of  $\alpha$ :

$$r_{\text{eff}} = r_0 \left( \frac{L_{\text{UV}}}{L_0} \right)^\alpha, \quad (1)$$

where  $L_{\text{UV}}$ , and  $L_0$  are the UV luminosity of galaxies, a fiducial UV luminosity we take as the  $z = 3$  characteristic luminosity, (i.e.,  $L_0 = L_{*,z=3}$ , corresponding to  $M_{\text{UV}} = -21$ ), respectively. Also,  $r_0$  is defined to be the size at  $L_0$ .

We derive the size-luminosity relation of our sample LAEs in Figure 2 by extending the previous analysis (e.g., Jiang et al. 2013; Kim et al. 2021) to fainter galaxies  $M_{\text{UV}} \simeq -14$ . We exclude the two highly magnified galaxies (A1689-1000 and A1689-1117) from the fit due to their large uncertainties in the magnification factor (i.e.,  $\sigma(\mu)/\mu > 1$ , see Table 1). The fitted slope and intercept are  $\alpha = 0.36 \pm 0.12$  and  $r_0 = 0.39^{+0.17}_{-0.12}$  kpc, respectively. The slope of our sample galaxies is broadly consistent, within uncertainties, with that of typical SFGs and LBGs at  $0.5 < z < 6$ , which show

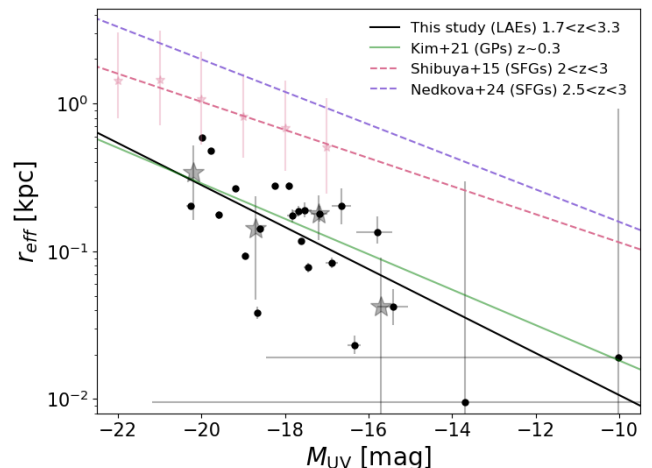


**Figure 2.** The UV size-luminosity relation for our sample of LAEs (black points) at  $1.7 < z < 3.3$  (Section 3.2). The black solid line represents the fitted relation for these galaxies, while the grey star points indicate the median sizes of our sample galaxies binned by UV luminosity. Light pink points and solid lines indicate the same relation for continuum-selected star-forming galaxies (SFGs) at similar redshifts (Shibuya et al. 2015), while the light purple relation is from (Nedkova et al. 2024). The green solid line represents the relation for local Green Pea galaxies ( $z \sim 0.3$ ), which are low-redshift analogs to high-redshift LAEs (Kim et al. 2021). At a given UV luminosity, our sample LAEs are smaller in size compared to typical SFGs, but they exhibit a size-luminosity relation similar to that of Green Pea galaxies, suggesting that LAEs maintain a consistently small size across redshifts.

a slope range of  $0.15 \lesssim \alpha \lesssim 0.5$ , with a typical value of  $\alpha \simeq 0.27$  (Grazian et al. 2012; Jiang et al. 2013; Huang et al. 2013; van der Wel et al. 2014; Shibuya et al. 2015;

Curtis-Lake et al. 2016; Kawamata et al. 2018; Nedkova et al. 2024).

In contrast to the slope  $\alpha$ , the intercept ( $r_0 = 390$  pc) of the size-luminosity relation for our sample LAEs is smaller than that observed for typical SFGs and LBGs ( $r_0 \simeq 1$  kpc). The small size of LAEs (at a fixed UV luminosity) leads to a high star formation surface density (i.e., star formation rate per unit area,  $\Sigma\text{SFR}$ ). We will further discuss how the high  $\Sigma\text{SFR}$  of LAEs is related to the escape of Ly $\alpha$  photons in Section 4.

### 3.3. The relation between UV size and the Ly $\alpha$ Equivalent Width

In this section, we investigate the possible correlations between UV size ( $r_{\text{eff}}$ ) and the Ly $\alpha$  equivalent width ( $\text{EW}(\text{Ly}\alpha)$ ) in our sample LAEs. We also compare the trends of our sample galaxies with those seen in other LAEs from the literature. Figure 3 shows the correlations between  $r_{\text{eff}}$  and  $\text{EW}(\text{Ly}\alpha)$ . There appears to be an anti-correlation between  $r_{\text{eff}}$  and  $\text{EW}(\text{Ly}\alpha)$ , with moderate scatter, where smaller galaxies tend to have *higher*  $\text{EW}(\text{Ly}\alpha)$ . While the small sample size may impact the reliability of the Spearman correlation test, leading to a weak correlation ( $p = 0.09$ , with  $p \leq 0.05$  considered significant), the mean  $\text{EW}(\text{Ly}\alpha)$  of the small size ( $r_{\text{eff}} < 0.1$  kpc) sub-sample galaxies is higher than that of the large size ( $r_{\text{eff}} \geq 0.1$  kpc) counterparts, which values of  $93 \pm 17$  Å and  $58 \pm 15$  Å, respectively.

A qualitatively similar anti-correlation between UV size and  $\text{EW}(\text{Ly}\alpha)$  has been found in other LAEs across a wide range of redshift ( $0.1 \lesssim z \lesssim 7$ ) (e.g., Bond et al. 2009, 2012; Guaita et al. 2015; Paulino-Afonso et al. 2018; Kim et al. 2021; Pucha et al. 2022; Reddy et al. 2022; Kerutt et al. 2022). Specifically, at redshifts  $z \simeq 2.1$  and  $3.1$  similar to our sample LAEs, Bond et al. (2012) showed that high  $\text{EW}(\text{Ly}\alpha)$  LAEs have a smaller median UV size compared to low  $\text{EW}(\text{Ly}\alpha)$  LAEs. Additionally, a linear-fit of the UV size and  $\text{EW}(\text{Ly}\alpha)$  relation for a sample of high- $z$  LAEs at  $2 \lesssim z \lesssim 6$ , as reported by Paulino-Afonso et al. (2018), reveals a negative slope of  $(-3.5 \pm 1.2) \times 10^{-3}$ . This result seems qualitatively consistent with the anti-correlation observed in our sample LAEs, where the linear fit between  $r_{\text{eff}}$  and  $\text{EW}(\text{Ly}\alpha)$  shows a negative slope of  $(-5.0 \pm 5.0) \times 10^{-4}$ .

At lower redshifts ( $0.03 < z < 0.2$ ), the Lyman alpha reference sample (LARS) reported a significant anti-correlation with the Spearman correlation coefficient ( $p$ -value) of  $-0.64$  (0.03) based on 12 local star-forming galaxies (Guaita et al. 2015). Similarly, Kim et al. (2021) reported a significant anti-correlation ( $p$ -value  $< 0.001$ ) between  $\text{EW}(\text{Ly}\alpha)$  and UV size based on

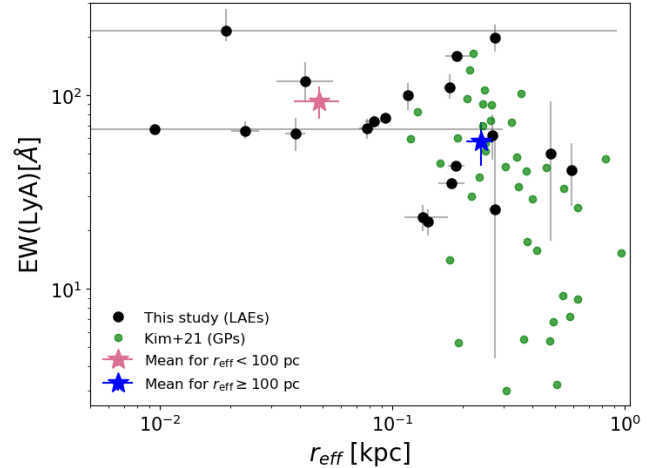


**Figure 3.** The figure illustrates the relation between Ly $\alpha$  emission equivalent width ( $\text{EW}(\text{Ly}\alpha)$ ) and UV-continuum size ( $r_{\text{eff}}$ ) for LAEs, with LAEs shown as black dots. The thick pink point represents the mean  $r_{\text{eff}}$  and  $\text{EW}(\text{Ly}\alpha)$  for the small-size sub-sample ( $r_{\text{eff}} < 100$  pc), while the blue point corresponds to the large-size sub-sample ( $r_{\text{eff}} \geq 100$  pc). The green points represent the relation for Green Pea galaxies (Kim et al. 2021) for comparison. The data distribution and median values indicate that smaller sizes are generally associated with higher  $\text{EW}(\text{Ly}\alpha)$ , which is consistent with previous studies (Section 3.3).

a sample of Green Pea galaxies. This suggests that a small size is preferred for significant Ly $\alpha$  emission.

## 4. DISCUSSION

### 4.1. Small Size and High $\Sigma\text{SFR}$ as a Crucial Condition for Ly $\alpha$ Escape

Our UV size analysis of LAEs at Cosmic Noon reveals that their sizes are approximately  $3\times$  smaller than those of continuum-selected SFGs and that they follow a distinct size-luminosity relation compared to typical SFGs. This is consistent with other studies analyzing the morphology of LAEs across a wide range of redshift ( $0.1 \lesssim z \lesssim 7$ ) (Malhotra et al. 2012; Jiang et al. 2013; Izotov et al. 2016, 2018a; Kim et al. 2020, 2021; Flury et al. 2022; Liu et al. 2023; Ning et al. 2024). Our analysis extends the LAE morphology analysis to faint UV luminosity ( $M_{\text{UV}} \simeq -14$ ).

Due to their small sizes, LAEs show a small intercept (i.e.,  $r_0 \simeq 0.4$  kpc, the size at  $M_{\text{UV}} = -21$  as in Eq. 1) in the size-luminosity relation, resulting in LAEs lying below the relation compared to their SFG counterparts (Section 3.2). Interestingly, the small  $r_0$  of our sample LAEs does not seem to follow the redshift evolution of  $r_0$  for continuum-selected SFGs and LBGs, but is instead consistent with that of low-redshift ( $z \sim 0.3$ ) LAEs (also known as Green Pea galaxies) (Izotov et al.

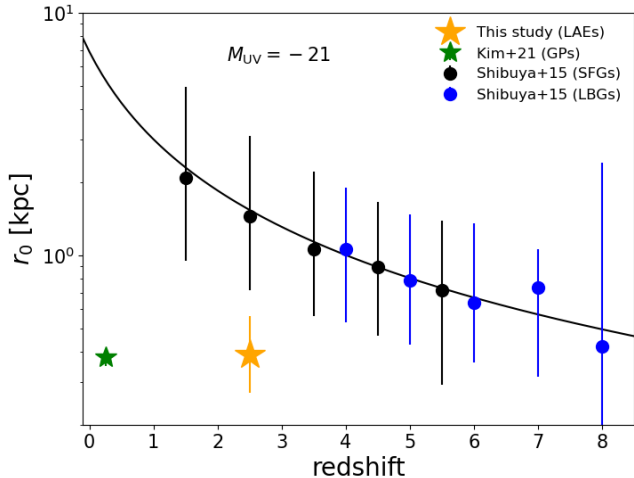


**Figure 4.** The intercept ( $r_0$ , size at  $M_{\text{UV}} = -21$ ) of the size-luminosity relation for our sample LAEs (indicated by the orange star) is distinctly smaller compared to that of typical (continuum-selected) star-forming galaxies at similar redshifts ( $\sim 0.4$  vs.  $\sim 1.5$  kpc), and does not seem to follow the expected redshift-dependent size growth seen in SFGs. For comparison, the  $r_0$  of Green Pea galaxies is shown as a green star, which closely matches the  $r_0$  of our sample LAEs at Cosmic Noon.

2016, 2018a; Kim et al. 2021; Flury et al. 2022). This is shown in Figure 4. The distinctly small intercept size  $r_0$  for the size-luminosity relations of LAEs both at low and high-redshift ( $z \sim 0.3$ – $3.5$ ) corroborates that LAEs have characteristic compact sizes independent of redshift (Malhotra et al. 2012; Jiang et al. 2013) and that the compact UV size likely plays a key role in the escape of  $\text{Ly}\alpha$  emission (Figure 3) (Kim et al. 2020, 2021).

Notably, the very small size of LAEs for a given UV luminosity results in concentrated star formation activity per unit area (that is, high star formation surface density,  $\Sigma\text{SFR}$ ), which is often associated with the presence of compact star-forming clumps within the galaxies (e.g., Keel 2005; Kim et al. 2020; Vanzella et al. 2022; Kim et al. 2023; Owens et al. 2024). Indeed, due to their high  $\Sigma\text{SFR}$ , LAEs are clearly separated from the typical SFGs in the diagram of  $\Sigma\text{SFR}$  vs. size, as shown in Figure 5. In the figure, we derive the SFR of our sample galaxies using the SFR-UV continuum flux relation from Kennicutt (1998), with the SFG counterparts taken from the 3D-HST survey (Skelton et al. 2014; Whitaker et al. 2014). Specifically, our sample LAEs with a mean  $r_{\text{eff}}$  of  $170 \pm 140$  pc show  $\Sigma\text{SFR} \gtrsim 1 M_{\odot} \text{ yr}^{-1} \text{ kpc}^{-2}$ , which is more than an order of magnitude higher than that of typical SFGs with similar UV luminosities and redshifts, as is clear from the lines of constant UV-magnitudes (e.g., Skelton et al. 2014; Whitaker et al. 2014). Consistent with our sample of LAEs, other LAEs from the

literature (i.e., Ritondale et al. 2019; Kim et al. 2021; Ning et al. 2024) also exhibit small sizes and high  $\Sigma\text{SFR}$ , occupying a distinct position in the  $\Sigma\text{SFR}$  vs.  $r_{\text{eff}}$  parameter space compared to SFGs.

Why do LAEs show small size ( $r_{\text{eff}} \lesssim 0.3$  kpc) and high  $\Sigma\text{SFR}$  ( $\gtrsim 1 M_{\odot} \text{ yr}^{-1} \text{ kpc}^{-2}$ ) compared to the SFG counterparts with similar UV luminosity, regardless of redshifts? Is the compact morphology of LAEs related to the escape of  $\text{Ly}\alpha$  photons? It has been suggested that a high  $\Sigma\text{SFR}$  indicates the presence of strong galactic outflows/winds. In this context, stellar winds and supernovae (SN) feedback in a dense starburst region generate significant radiation pressure, resulting in a galactic-scale outflow. (e.g., Meurer et al. 1997; Heckman 2001a; Heckman et al. 2001b, 2015; Alexandroff et al. 2015; Heckman & Borthakur 2016; Sharma et al. 2017; Cen 2020; Menon et al. 2024). Indeed,  $\Sigma\text{SFR}$  shows a positive correlation with gas pressure in HII regions (Meurer et al. 1997; Kim et al. 2011; Jiang et al. 2019b), high ionization states (i.e., O32 line ratio), and electron density (Reddy et al. 2023a,b), suggesting that high  $\Sigma\text{SFR}$  is closely connected to the extreme ISM conditions resulting from galactic outflows.

Considering  $\Sigma\text{SFR}$  threshold of  $> 0.1 M_{\odot} \text{ yr}^{-1} \text{ kpc}^{-2}$  for having galactic outflows, as suggested by Heckman (2001a); Sharma et al. (2017), it is notable that all of our sample LAEs exceed this threshold, as shown in Figure 5. Furthermore, most of our sample LAEs, along with others from the literature, have  $\Sigma\text{SFR}$  values well above this threshold, typically exceeding  $\Sigma\text{SFR} \gtrsim 1 M_{\odot} \text{ yr}^{-1} \text{ kpc}^{-2}$ . This indicates the presence of strong galactic outflows in LAEs across a range of redshifts.

Strong galactic outflows have been considered as one of the promising mechanisms to create under-dense channels in the ISM for the escape of  $\text{Ly}\alpha$  and potentially  $\text{LyC}$  photons (Keel 2005; Borthakur et al. 2014; Alexandroff et al. 2015; Mainali et al. 2022; Amorín et al. 2024). Indeed Green Pea galaxies—which are low-redshift ( $z \sim 0.3$ ) LAEs—are characterized with compact morphology (high  $\Sigma\text{SFR}$ ) (Kim et al. 2021), and show high gas pressure (Jiang et al. 2019b) and outflows (Amorín et al. 2024). Notably, Kim et al. (2020) demonstrated direct correlations between central  $\Sigma\text{SFR}$  (and specific  $\Sigma\text{SFR}$ ,  $\Sigma\text{sSFR} = \Sigma\text{SFR}/M_{\text{star}}$ ) and the  $\text{Ly}\alpha$  emission line properties. They found significant correlations between  $\Sigma\text{sSFR}$  and  $\text{EW}(\text{Ly}\alpha)$  and  $\text{Ly}\alpha$  escape fraction, suggesting that an intense central starburst can drive galactic outflows in galaxies with shallow gravitational potential wells, thus clearing channels for the escape of  $\text{Ly}\alpha$  photons. Qualitatively consistent conclusions on the importance of  $\Sigma\text{SFR}$  and specific  $\Sigma\text{SFR}$  on the escape of  $\text{Ly}\alpha$  and  $\text{LyC}$  have been reported based on stud-

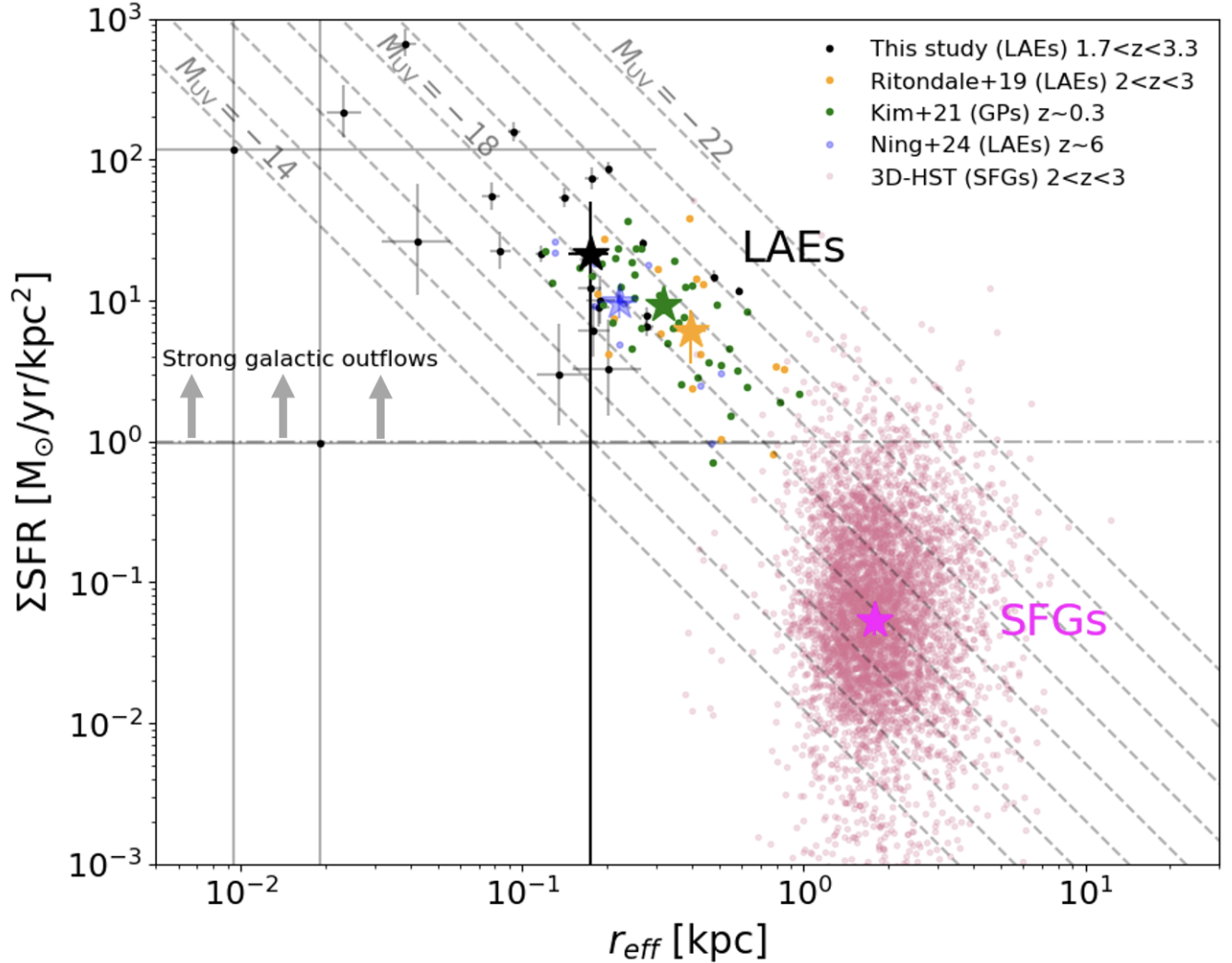


**Figure 5.** The Star Formation Surface Density ( $\Sigma\text{SFR}$ ) vs. Size ( $r_{\text{eff}}$ ) relation for LAEs compared to typical star-forming galaxies (SFGs) is shown. The black circles represent our sample of LAEs, with the median denoted by the black star. LAEs from the literature, spanning a redshift range of  $0.3 \lesssim z \lesssim 6$  (Ritondale et al. 2019; Kim et al. 2021; Ning et al. 2024), are plotted as green, blue, and orange points. For comparison, typical SFGs from the 3D-HST survey are shown as pink points (Skelton et al. 2014; Whitaker et al. 2014). The dashed lines correspond to constant UV luminosity, ranging from  $M_{\text{UV}} = -22$  to  $M_{\text{UV}} = -14$ . The dot-dashed horizontal line marks an empirical  $\Sigma\text{SFR}$  threshold of  $= 1 M_{\odot} \text{ yr}^{-1} \text{ kpc}^{-2}$ , with the majority of LAEs lying above this threshold, indicating strong galactic outflows (Section 4.1). Given their small size for a given UV luminosity, LAEs are characterized by compact morphologies and exhibit significantly higher  $\Sigma\text{SFR}$  compared to typical SFGs—by two orders of magnitude. This suggests that compact morphology plays a crucial role in facilitating the escape of Ly $\alpha$  photons. Additionally, the distinctive location of LAEs in the  $\Sigma\text{SFR}$  vs. size diagram can be used to identify potential Ly $\alpha$ -emitters.

ies of Green Pea galaxies and LAEs at  $1.8 \lesssim z \lesssim 3.5$  (e.g., Reddy et al. 2022; Flury et al. 2022; Pucha et al. 2022; Jaskot et al. 2024).

The presence of strong outflows and the clearing of channels in the ISM for Ly $\alpha$  escape are further supported by the weak low-ionization interstellar (LIS) absorption lines observed in our sample LAEs (Snapp-Kolas et al. 2024) as well as other LAEs (e.g., Shapley et al. 2003; Steidel et al. 2011; Henry et al. 2015), as

LIS absorption lines serve as an effective tracer of the neutral hydrogen covering fraction.

Our results on the compact UV size and high  $\Sigma\text{SFR}$  of a sample of 23 LAEs at Cosmic Noon emphasize the importance of compact morphology on the escape of Ly $\alpha$  photons, in agreement with galactic outflow-driven Ly $\alpha$  escape mechanisms.

## 5. SUMMARY AND CONCLUSIONS

We investigate the UV-continuum size and luminosity of a sample of 23 Ly $\alpha$ -emitters at  $1.7 < z < 3.3$ . Using



deep, high-resolution HST imaging combined with gravitational lensing from a foreground galaxy cluster, we can robustly measure the morphology of our sample galaxies down to faint UV luminosities ( $M_{\text{UV}} \simeq -14$ ) at Cosmic Noon. We compare the sizes of these LAEs with those of continuum-selected star-forming galaxies (SFGs) at similar redshifts. Our analysis reveals that the average size of LAEs is distinctly smaller than that of typical SFGs, reinforcing previous findings of the characteristic small size of LAEs, which appears to be independent of redshift.

Our primary conclusions are summarized below.

- Our sample of LAEs exhibits very small sizes, with a mean effective radius ( $r_{\text{eff}}$ ) of 170 pc. The size distribution (Figure 1) is narrow, with a standard deviation of 140 pc, though there is a long tail toward larger sizes (up to  $\simeq 600$  pc). Compared to continuum-selected normal SFGs at similar redshifts, the typical sizes of our LAEs are approximately a factor of  $\sim 3$  smaller at a given UV luminosity (Section 3.1). The small sizes observed in our sample are consistent with those of LAEs at similar redshifts, as well as with low-redshift Green Pea galaxies. This suggests that the compact morphology and small sizes of LAEs play a key role in facilitating the escape of Ly $\alpha$  photons.
- The UV size-luminosity relation of LAEs (Figure 2) shows a fitted slope of  $0.36 \pm 0.12$  and an intercept of  $r_0 = 0.39^{+0.17}_{-0.12}$  kpc measured at  $M_{\text{UV}} = -21$ . The slope is slightly higher than the average slope values of typical star-forming galaxies at low and high redshifts, within the uncertainties (i.e.,  $0.15 \lesssim \alpha \lesssim 0.5$ ).
- Unlike typical SFGs, the intercept  $r_0$  of LAEs does not show the expected size growth with decreasing redshift (Figure 4). Specifically, LAEs have an  $r_0$  that is approximately  $3\times$  smaller than that of SFGs at similar redshifts. This smaller  $r_0$  is consistent with the sizes observed in low- $z$  Green Pea galaxies (i.e., low- $z$  LAEs), suggesting that LAEs maintain compact, non-evolving sizes regardless of redshift.
- There is an anti-correlation between UV-continuum size ( $r_{\text{eff}}$ ) and EW(Ly $\alpha$ ) (Figure 3),

where EW(Ly $\alpha$ ) decreases as  $r_{\text{eff}}$  increases. This trend is consistent with previous studies of LAEs across a wide redshift range ( $0.1 < z < 6$ ), suggesting that a compact size is favorable for significant Ly $\alpha$  emission.

- Due to their compact size for a given UV luminosity, our sample of LAEs exhibits high  $\Sigma\text{SFR}$  ( $1\text{--}600 M_{\odot} \text{ yr}^{-1} \text{ kpc}^{-2}$ ), which is more than two orders of magnitude higher than that of continuum-selected SFGs at similar redshifts. With a  $\Sigma\text{SFR}$  threshold of  $> 0.1 M_{\odot} \text{ yr}^{-1} \text{ kpc}^{-2}$  for galactic outflows, our sample LAEs surpass this threshold, indicating strong outflows in these galaxies. Moreover, other LAEs in the literature show similar small sizes and high  $\Sigma\text{SFR}$  values, reinforcing the trend.

We find that LAEs occupy a distinct region in the  $\Sigma\text{SFR}$  vs.  $r_{\text{eff}}$  diagram, with most LAEs having smaller sizes and higher  $\Sigma\text{SFR}$  for a given UV luminosity compared to SFG counterparts (Figure 5). This suggests that the  $\Sigma\text{SFR}$  vs. size relationship can be a useful tool for identifying Ly $\alpha$ -emitters.

In conclusion, our results suggest that compact morphology and high  $\Sigma\text{SFR}$  are key factors in enabling Ly $\alpha$  (and potentially LyC) photon escape, as they create favorable conditions for strong galactic outflows. These outflows, likely driven by stellar feedback and/or supernovae from concentrated starburst regions, create under-dense channels that facilitate Ly $\alpha$  escape.

Our study implies that small sizes for a given luminosity can be an effective criterion for selecting Ly $\alpha$ -emitters.

- 1 KJK thanks Yu-Heng Lin, Sangeeta Malhotra, and
- 2 James E. Rhoads for their useful discussions on this
- 3 study. Support for this work was provided by awards
- 4 HST-GO-15940 from STScI, which is operated by
- 5 AURA, Inc. for the National Aeronautics Space Ad-
- 6 ministration (NASA) under contract NAS 5-26555.

*Facilities:* HST(ACS/WFC)

*Software:* astropy (??)

## REFERENCES

- Ahn, S.-H., Lee, H.-W., & Lee, H. M. 2003, MNRAS, 340, 863
- Alavi, A., Siana, B., Richard, J., et al. 2014, ApJ, 780, 143
- Alavi, A., Siana, B., Richard, J., et al. 2016, ApJ, 832, 56

- Alexandroff, R. M., Heckman, T. M., Borthakur, S., et al. 2015, *ApJ*, 810, 104
- Amorín, R. O., Rodríguez-Henríquez, M., Fernández, V., et al. 2024, *A&A*, 682, L25
- Barnes, J., & Efstathiou, G. 1987, *ApJ*, 319, 575
- Bond, N. A., Gawiser, E., Gronwall, C., et al. 2009, *The Astrophysical Journal*, 705, 639
- Bond, N. A., Gawiser, E., Guaita, L., et al. 2012, *ApJ*, 753, 95
- Borthakur, S., Heckman, T. M., Leitherer, C., et al. 2014, *Science*, 346, 216
- Bouwens, R. J., Illingworth, G. D., Blakeslee, J. P., et al. 2004, *ApJL*, 611, L1
- Cen, R. 2020, *ApJL*, 889, L22
- Chang, S.-J., Yang, Y., Seon, K.-I., et al. 2023, *ApJ*, 945, 100
- Curtis-Lake, E., McLure, R. J., Dunlop, J. S., et al. 2016, *MNRAS*, 457, 440
- de Barros, S., Vanzella, E., Amorín, R., et al. 2016, *Astronomy and Astrophysics*, 585, A51
- Diolaiti, E., Bendinelli, O., Bonaccini, D., et al. 2000, in *ASP Conf. Ser. 216, Astronomical Data Analysis Software and Systems IX*, ed. N. Manset, C. Veillet, & D. Crabtree (San Francisco, CA: ASP), 623
- Dow-Hygelund, C. C., Holden, B. P., Bouwens, R. J., et al. 2007, *ApJ*, 660, 47
- Fall, S. M., & Efstathiou, G. 1980, *MNRAS*, 193, 189
- Finkelstein, K. D., Finkelstein, S. L., Tilvi, V., et al. 2015, *ApJ*, 813, 78
- Finkelstein, S. L., Ryan, R. E., Papovich, C., et al. 2015, *ApJ*, 810, 71. doi:10.1088/0004-637X/810/1/71
- Flury, S. R., Jaskot, A. E., Ferguson, H. C., et al. 2022, *ApJ*, 930, 126
- Gawiser, E., Francke, H., Lai, K., et al. 2007, *ApJ*, 671, 278
- Gazagnes, S., Chisholm, J., Schaerer, D., et al. 2020, *arXiv e-prints*, arXiv:2005.07215
- Grazian, A., Castellano, M., Fontana, A., et al. 2012, *A&A*, 547, A51
- Gronwall, C., Bond, N. A., Ciardullo, R., et al. 2011, *ApJ*, 743, 9
- Guaita, L., Melinder, J., Hayes, M., et al. 2015, *A&A*, 576, A51
- Hathi, N. P., Le Fèvre, O., Ilbert, O., et al. 2016, *A&A*, 588, A26
- Heckman, T. M. & Borthakur, S. 2016, *ApJ*, 822, 9
- Heckman, T. M., Alexandroff, R. M., Borthakur, S., et al. 2015, *ApJ*, 809, 147
- Heckman, T. M., Sembach, K. R., Meurer, G. R., et al. 2001b, *ApJ*, 558, 56. doi:10.1086/322475
- Heckman, T. M. 2001, *Gas and Galaxy Evolution*, 240, 345
- Henry, A., Scarlata, C., Martin, C. L., et al. 2015, *ApJ*, 809, 19
- Huang, K.-H., Ferguson, H. C., Ravindranath, S., et al. 2013, *ApJ*, 765, 68
- Izotov, Y. I., Schaerer, D., Thuan, T. X., et al. 2016, *MNRAS*, 461, 3683
- Izotov, Y. I., Schaerer, D., Worseck, G., et al. 2018a, *MNRAS*, 474, 4514
- Izotov, Y. I., Worseck, G., Schaerer, D., et al. 2018b, *MNRAS*, 478, 4851
- Izotov, Y. I., Worseck, G., Schaerer, D., et al. 2021, *MNRAS*, 503, 1734
- Jaskot, A. E., Silveyra, A. C., Plantinga, A., et al. 2024, *ApJ*, 972, 92
- Jauzac, M., Richard, J., Limousin, M., et al. 2016, *MNRAS*, 457, 2029. doi:10.1093/mnras/stw069
- Jiang, L., Egami, E., Fan, X., et al. 2013, *ApJ*, 773, 153
- Jiang, T., Malhotra, S., Yang, H., et al. 2019b, *ApJ*, 872, 146
- Kawamata, R., Ishigaki, M., Shimasaku, K., et al. 2018, *ApJ*, 855, 4
- Keel, W. C. 2005, *AJ*, 129, 1863. doi:10.1086/428371
- Kerutt, J., Wisotzki, L., Verhamme, A., et al. 2022, *A&A*, 659, A183
- Kim, C.-G., Kim, W.-T., & Ostriker, E. C. 2011, *ApJ*, 743, 25
- Kim, K. J., Bayliss, M. B., Rigby, J. R., et al. 2023, *ApJL*, 955, L17. doi:10.3847/2041-8213/acf0c5
- Kim, K., Malhotra, S., Rhoads, J. E., et al. 2020, *ApJ*, 893, 134
- Kim, K. J., Malhotra, S., Rhoads, J. E., et al. 2021, *ApJ*, 914, 2
- Kim, K., Oh, S., Jeong, H., et al. 2016, *ApJS*, 225, 6
- Kennicutt, R. C. 1998, *ARA&A*, 36, 189. doi:10.1146/annurev.astro.36.1.189
- Limousin, M., Richard, J., Jullo, E., et al. 2007, *ApJ*, 668, 643. doi:10.1086/521293
- Limousin, M., Richard, J., Jullo, E., et al. 2016, *A&A*, 588, A99. doi:10.1051/0004-6361/201527638
- Liu, C., Mutch, S. J., Poole, G. B., et al. 2017, *MNRAS*, 465, 3134
- Liu, Y., Dai, Y. S., Wuyts, S., et al. 2023, *arXiv:2309.11559*. doi:10.48550/arXiv.2309.11559
- Lotz, J. M., Koekemoer, A., Coe, D., et al. 2017, *ApJ*, 837, 97. doi:10.3847/1538-4357/837/1/97
- Mainali, R., Rigby, J. R., Chisholm, J., et al. 2022, *ApJ*, 940, 160
- Malhotra, S., & Rhoads, J. E. 2002, *ApJL*, 565, L71
- Malhotra, S., Rhoads, J. E., Finkelstein, S. L., et al. 2012, *ApJL*, 750, L36

- Meurer, G. R., Heckman, T. M., Lehnert, M. D., Leitherer, C., & Lowenthal, J. 1997, *AJ*, 114, 54
- Menon, S. H., Burkhart, B., Somerville, R. S., et al. 2024, arXiv:2408.14591. doi:10.48550/arXiv.2408.14591
- Mo, H. J., Mao, S., & White, S. D. M. 1998, *MNRAS*, 295, 319
- Morishita, T., Stiavelli, M., Chary, R.-R., et al. 2024, *ApJ*, 963, 9
- Nedkova, K. V., Rafelski, M., Teplitz, H. I., et al. 2024, arXiv:2405.10908. doi:10.48550/arXiv.2405.10908
- Ning, Y., Cai, Z., Lin, X., et al. 2024, *ApJL*, 963, L38
- Neufeld, D. A. 1991, *ApJL*, 370, L85
- Overzier, R. A., Bouwens, R. J., Cross, N. J. G., et al. 2008, *ApJ*, 673, 143
- Owens, M. R., Kim, K. J., Bayliss, M. B., et al. 2024, arXiv:2410.03660
- Oyarzún, G. A., Blanc, G. A., González, V., et al. 2017, *ApJ*, 843, 133
- Pahl, A. J., Shapley, A., Steidel, C. C., et al. 2021, *MNRAS*, 505, 2447
- Paulino-Afonso, A., Sobral, D., Ribeiro, B., et al. 2018, *MNRAS*, 476, 5479
- Peng, C. Y., Ho, L. C., Impey, C. D., et al. 2002, *AJ*, 124, 266
- Peng, C. Y., Ho, L. C., Impey, C. D., et al. 2010, *AJ*, 139, 2097
- Pirzkal, N., Malhotra, S., Rhoads, J. E., et al. 2007, *ApJ*, 667, 49
- Pucha, R., Reddy, N. A., Dey, A., et al. 2022, *AJ*, 164, 159
- Reddy, N. A. & Steidel, C. C. 2009, *ApJ*, 692, 778. doi:10.1088/0004-637X/692/1/778
- Reddy, N. A., Topping, M. W., Shapley, A. E., et al. 2022, *ApJ*, 926, 31
- Reddy, N. A., Sanders, R. L., Shapley, A. E., et al. 2023, *ApJ*, 951, 56
- Reddy, N. A., Topping, M. W., Sanders, R. L., et al. 2023, *ApJ*, 952, 167
- Rhoads, J. E., Malhotra, S., Dey, A., et al. 2000, *ApJ*, 545, L85
- Rhoads, J. E., Malhotra, S., Richardson, M. L. A., et al. 2014, *ApJ*, 780, 20
- Ribeiro, B., Le Fèvre, O., Tasca, L. A. M., et al. 2016, *A&A*, 593, A22
- Ritondale, E., Auger, M. W., Vegetti, S., et al. 2019, *MNRAS*, 482, 4744
- Rivera-Thorsen, T. E., Dahle, H., Gronke, M., et al. 2017, *A&A*, 608, L4
- Sérsic, J. L. 1968, *Atlas de Galaxies Australes (Córdoba: ObS, Astron., Univ. Nac. Córdoba)*
- Shapley, A. E., Steidel, C. C., Pettini, M., et al. 2003, *ApJ*, 588, 65. doi:10.1086/373922
- Sharma, M., Theuns, T., Frenk, C., et al. 2017, *MNRAS*, 468, 2176
- Sharon, K., Mahler, G., Rivera-Thorsen, T. E., et al. 2022, *ApJ*, 941, 203
- Shen, S., Mo, H. J., White, S. D. M., et al. 2003, *MNRAS*, 343, 978
- Shibuya, T., Ouchi, M., & Harikane, Y. 2015, *ApJS*, 219, 15
- Shibuya, T., Ouchi, M., Harikane, Y., et al. 2019, *ApJ*, 871, 164
- Skelton, R. E., Whitaker, K. E., Momcheva, I. G., et al. 2014, *ApJS*, 214, 24
- Snapp-Kolas, C., Siana, B., Gburek, T., et al. 2023, *MNRAS*, 525, 5500
- Snapp-Kolas, C., Siana, B., Gburek, T., et al. 2024, arXiv:2401.05498
- Steidel, C. C., Bogosavljević, M., Shapley, A. E., et al. 2011, *ApJ*, 736, 160
- Steidel, C. C., Bogosavljević, M., Shapley, A. E., et al. 2018, *ApJ*, 869, 123
- Taniguchi, Y., Murayama, T., Scoville, N. Z., et al. 2009, *ApJ*, 701, 915
- van der Wel, A., Bell, E. F., Häussler, B., et al. 2012, *ApJS*, 203, 24. doi:10.1088/0067-0049/203/2/24
- van der Wel, A., Franx, M., van Dokkum, P. G., et al. 2014, *ApJ*, 788, 28
- Vanzella, E., Castellano, M., Bergamini, P., et al. 2022, *A&A*, 659, A2. doi:10.1051/0004-6361/202141590
- Verhamme, A., Orlitová, I., Schaerer, D., et al. 2015, *Astronomy and Astrophysics*, 578, A7
- Whitaker, K. E., Franx, M., Leja, J., et al. 2014, *ApJ*, 795, 104
- Wyithe, J. S. B., & Loeb, A. 2011, *MNRAS*, 413, L38